Experimental Investigation of Small Scale Transport Mechanisms in the Stratosphere

N. W. ROSENBERG,* R. E. GOOD,† W. K. VICKERY,‡ AND E. M. DEWAN†
Air Force Cambridge Research Laboratories, L. G. Hanscom Field, Bedford, Mass.

Transport properties in the stratosphere were measured in an experimental program where smoke trails, deposited by rockets and aircraft, were recorded by time-lapse photography. This allowed winds, wind shears, and the rate of dispersion of the smoke to be calculated. Radial growth of the trails conformed to a turbulent diffusion rate; the effective diffusion coefficient at 20 km was approximately 0.7 m^2/sec. The spatial turbulence structure was determined from measured wind shears. Average energy spectra were obtained for total vertical profiles and segmented profiles of horizontal winds. A consistent finding was that the energy spectrum dependence exponent was close to $n = -2.8$. In the case of segmented profile spectra we found that 20% of the sample population showed $n < 2.2$ (indicating an inertial subrange). This is consistent with the presence of intermittent thin layers of efficient mixing in the 5–18 km height range. We also found an increase of wind shear and amplitude with altitude in this region.

Nomenclature

A = drag reference area
C_D = drag coefficient
f = L/λ where f is a positive integer and L is the total trail length
g = acceleration of gravity
k = wave number (spatial frequency)
K = eddy diffusion coefficient
n = frequency exponent
P = energy spectrum
r = full radius of turbulent wake
R = Gaussian radius
Ri = Richardson number
S = aircraft wingspan
t = time
T = temperature
v = velocity
w = aircraft weight
x, y, z = coordinates
X = distance downstream of vehicles
β = proportionality constant of Prandtl mixing length to wake width
ε = mean dissipation rate
Γ = dry adiabatic lapse rate (9.9°/km)
ϕ = smoke concentration
λ = wavelength
ρ = atmospheric density

Subscripts

$( )_b$ = rocket body
$( )_o$ = initial value
$( )_N$ = Nyquist

1. Introduction

THE objectives of this experimental program were to measure simultaneously the vertical profiles of the horizontal wind, temperature, and the radial growth of tracers at stratospheric altitudes. The measurements were directed toward a better understanding of transport mechanisms in the stratosphere; in particular, the rate of mixing and diffusion of exhaust products into the stratosphere. Diffusion coefficients were directly estimated from the radial growth of rocket and aircraft trails. To complement such measurements, lower bounds can be estimated, under certain conditions, from spatial frequency spectra of winds, temperatures, and density fluctuations along the tracer trail. This can only be done when the spectra reveal an inertial subrange over a region of k. This was one of our original motives for obtaining such spectra (see Appendix). However, for reasons to be given below, our data did not permit this approach to be used here. Thus, actual application of this technique must be deferred to a future report. The energy spectra, however, were found useful in other ways, as will be seen.

2. Tracer Releases

Miller et al.[1] obtained several stratospheric wind profiles by forming smoke along a rocket trajectory. They photographed the white smoke formed by hydrolysis of released liquid $TiCl_4$ with ambient water vapor. They also reported a few trails made to altitudes above 20 km by the simultaneous release of $TiCl_4$ and liquid water. We adopted this dual release method in a series of three launches from White Sands Missile Range on Feb. 2, 1973. The smoke trails covered the altitude range from 15 to 24 km. A montage of time lapse photography is shown in Fig. 1.

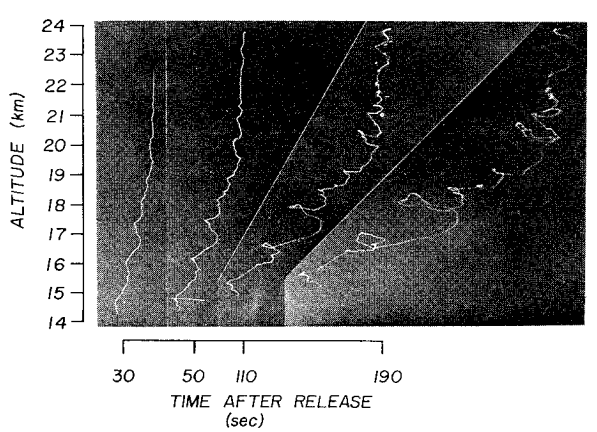

Fig. 1 Rocket smoke trails: distortion over time.

Presented as Paper 73-496 at the AIAA/AMS International Conference on the Environmental Impact of Aerospace Operators in the High Atmosphere, Denver, Colo., June 11–13, 1973; submitted July 6, 1973; revision received February 20, 1974. We thank S. P. Zimmerman, A. F. Quesada, D. Golomb, and V. L. Corbin for discussions and help in analysis of the data.

Index categories: Atmospheric, Space, and Oceanographic Sciences; Jets, Wakes, and Viscid-Inviscid Flow Interactions.

* Branch Chief, Chemical Physics Branch, Aeronomy Laboratory.
† Research Physicist (Atmospheric).
‡ Supervisory Aerospace Engineer. Member AIAA.

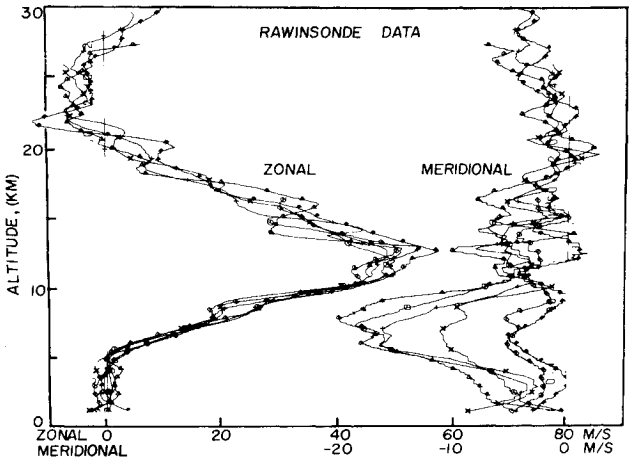

Fig. 2 Wind profile from Rawinsonde data.

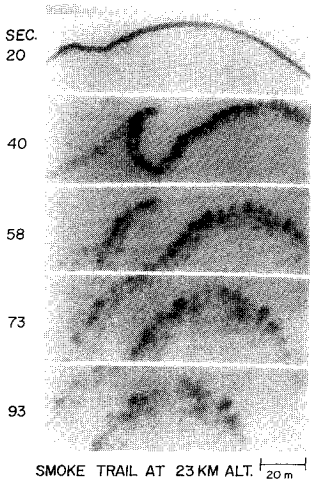

Fig. 4 Section of rocket smoke trail: distortion over time.

In this figure, the distortion of the smoke trail clearly revealed the strong wind field and vertical shears of the horizontal wind.

In addition to the smoke drift measurements, meteorological sounding balloons were launched almost simultaneously. The balloon-measured stratospheric winds are shown in Fig. 2. Tropospheric data from Jimspheres (2 m, spherical balloons with devices to prevent vortex shedding) are shown in Fig. 3. Similar $TiCl_4$ tracer releases from an aircraft were scheduled but venting failure prevented the $TiCl_4$ release and a fuel (kerosene) dump was substituted. The fuel dumps at 17 and 18.5 km altitude coincided in time with other measurements so that atmospheric wind and temperature structure were known at these locations. The fuel release of 10 kg/sec from an aircraft flying with a velocity of 200 m/sec (50 g/m) was photographed for about 200 sec. The $TiCl_4$–H_2O release at 1 kg/sec from a rocket flying at 1 km/sec (1 g/m) was photographed for 600 sec. Thus the kerosene was 100 times less effective for scattering sunlight, which was probably due to a 100-fold larger particle size obtained from fuel compared to the 2 μ $TiCl_4$ smoke particles. The $TiCl_4$ dispense rate provided an optical thickness of unity with an initial trail diameter of 0.5 m and a brightness 10% above sky background at a trail diameter of about 50 m.

The trails were photographed from several sites with cameras of focal lengths ranging from 50 mm to 1600 mm. Trail triangulation used 500 mm focal length camera records (Fig. 1) with a field of view of 15 × 15 km at the trail. Figures 2, 3, 8, and 9 are based on data obtained by R. O. Olsen et al.[2] at the White Sands Missile Range, U.S. Army.

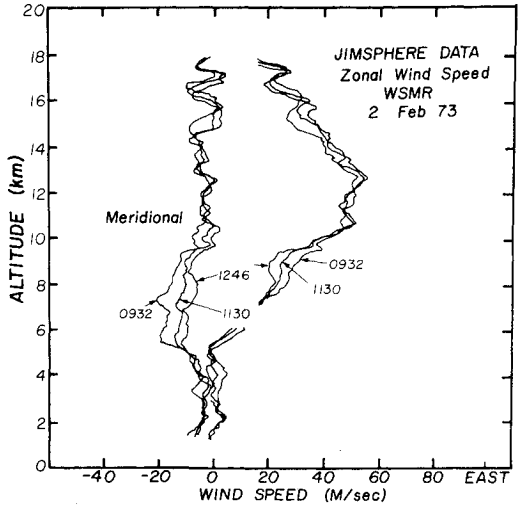

Fig. 3 Wind profiles for Jimsphere data.

White Sands Missile Range provided excellent phototheodolite coverage (1270 mm focal length) as shown in Figs. 4 and 5. Figure 5 contains three side view (elevation angle 28°) photographs of the fuel dump at 17 km. The fuel was dumped from a WB-57F aircraft in two streams, each at 10 kg/sec. From Fig. 5b, it is seen that the fuel droplets descended at an initial rate of approximately 3 m/sec. Figure 5c indicates that the main portion of the fuel dump dropped 60 m leaving a visible residue behind it.

3. Radial Growth

The radial growth of the smoke trail can be caused by 1) atmospheric diffusion, and 2) turbulent wake expansion. The growth due to diffusion is defined by

$$\partial\phi/\partial t = K\nabla^2\phi \qquad (1)$$

Assuming that the initial concentration is gaussion as a function of trail radius, it is known[3] that the "gaussian radius," R, depends on time as $R^2 = R_o^2 + 4Kt$ where R_o is the initial radius. Thus the effective diffusion coefficient K can be obtained from the slope of the plot R^2 vs time.

In order to measure the radial growth of both the fuel dump and smoke trails, an interactive computer controlled densitometer,[4] was employed. Photographs shown in Figs. 4 and 5 were scanned and a digital record of density was stored onto a disk. These film densities were converted to line of sight brightnesses and the background was subtracted. Next, the trail images were "unbent" to provide the straightened images shown in Fig. 6. Going from left to right in this figure we pass from earlier to later times of the same piece of trail. As time passed, progressively more trail straightening had to be done. The trail radius (also) increased with time as did the lumpy nature of the trail. In order to cope with this irregular, lumpy quality, it was

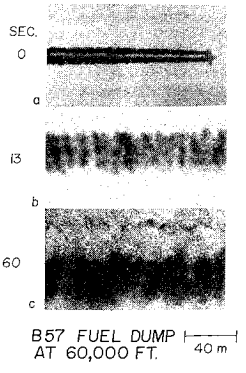

Fig. 5 Section of aircraft fuel dump trail: distortion over time.

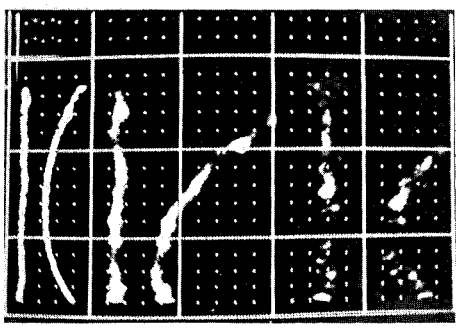

Fig. 6 Densitometer images: "unbent by computer manipulation of stored images (time from left to right). The left member of each of the 3 pairs is the straightened image.

necessary to compute the radial distribution by summing brightness over a series of lines parallel to the trail. The measurement was made line by line across the diameter of the trail, and provided an integrated radial distribution of object density, from which estimates of gaussian widths were made. The gaussian radii were plotted in Fig. 7. Initial radii grew from approximately 3 m to approximately 17 m over 130 sec. These growth rates lead to computed diffusivities of 0.7 m^2/sec from the rocket and 0.8 m^2/sec from the aircraft, about 100-fold greater than molecular values. Of course, it is crucial to show that this diffusivity is due to ambient turbulence and not to wake effects.

The rocket itself, which was not thrusting during smoke release, generated a turbulent wake as it passed through the atmosphere. Axisymmetric wakes are known[5] to grow in width as $X^{1/3}$. Thus as an order of magnitude estimate, assuming an initial wake diameter equal to the body diameter, the rocket turbulent wake radius can be represented as

$$r/r_b = (X/r_b)^{1/3} \tag{2}$$

A more precise representation of the wake dimension was given by Chang[6]

$$r = (134)^{1/3}\beta^{2/3}(C_D AX)^{1/3}/2 \tag{3}$$

Schlichting[7] reports $\beta = 0.18$ for two-dimensional wakes. The $C_D A$ parameter was obtained by matching the drag equation to the observed trajectory. At the altitude of interest, $C_D A = 0.085$ m^2. For an area based on the body diameter of 0.41 m, $C_D = 0.64$.

The two equations for rocket wake radius agree within 5%. The rocket velocity of about 66 m/sec, which is nearly horizontal

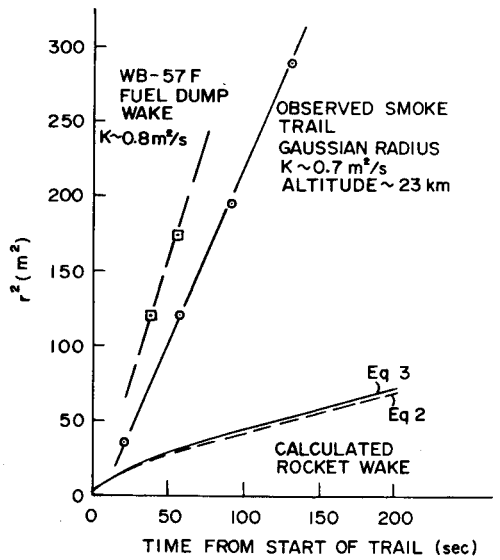

Fig. 7 Radial growth of trails with time, and theoretical growth of rocket wake.

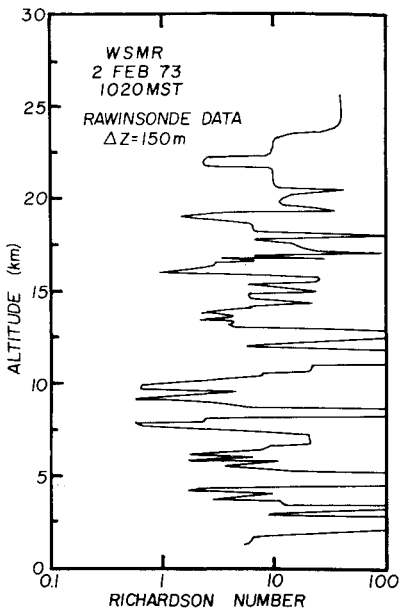

Fig. 8 Richardson number vs altitude from Rawinsonde data.

as the rocket passes over apogee, was used to evaluate X as a function of time. The predicted full radius of the rocket's turbulent wake is shown in Fig. 7. It is seen that the rocket turbulent wake has negligible effect on the growth of the smoke trail gaussian radius. It is therefore concluded that $K = 7 \times 10^3$ cm^2/sec represents the actual atmospheric vertical diffusivity.

Our estimates of diffusivity are comparable with some of the measurements already reported at these altitudes,[8] $K \sim 10^3 - 10^4$ cm^2/sec. It should be emphasized that the above mentioned diffusion rate was taken at only 1 altitude in a region where there was no high shear present at the time.

In the case of the aircraft, one can determine the time interval of the wake vortex regime[9] by $2 < t/\tau < 10$ where $\tau = \rho v S^3/w$. The values were: $w = 26{,}928$ kg, $S = 37.3$ m, $\rho = 1.42 \times 10^{-1}$ kg/m^3, $v = 200$ m/sec. Thus the wake vortex regime occurred in the interval $11 < t < 55$ sec and hence it dominated the dispersion of the fuel dump. Consequently, the diffusivity measured in this way is not valid. Subsequent observations of aircraft wakes have been observed for 30 min and may provide reliable diffusivities.

4. Atmospheric Stability

Since we were concerned with the determination of turbulent regions, we were interested in the stability profile of the atmosphere. A measure of stability of a stratified fluid in a gravitational

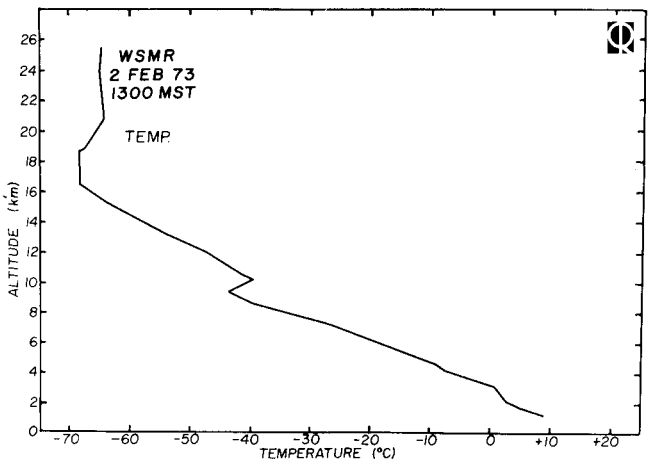

Fig. 9 Temperature profile.

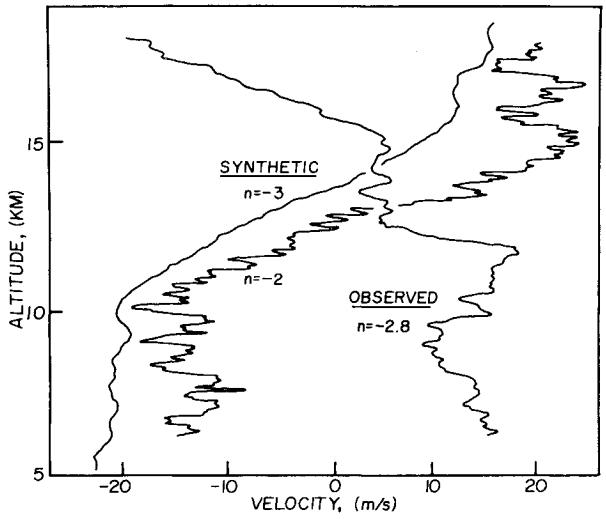

Fig. 10 Exponent n as measure of fine structure: synthetic and real wind profiles.

field is given by the Richardson number which is defined as the ratio of the square of the buoyancy (Brunt-Väisälä) frequency to the square of the vertical shear in the horizontal velocity.

$$Ri = \frac{(g/T)[(\partial T/\partial z)+\Gamma]}{[(\partial v_x/\partial z)^2+(\partial v_y/\partial z)^2]} \tag{4}$$

The Richardson number profile as determined from Rawinsonde balloon data taken at 1020 MST is shown in Fig. 8. The temperature profile (Fig. 9) was provided by the White Sands Missile Range.[2] This figure shows the tropopause at 16 km with a slight inversion at 10 km (double tropopause).

When $Ri < \frac{1}{4}$, free shear flows of the type considered here become unstable.[11,12] As can be seen from Fig. 8 the stratosphere and upper troposphere were on the whole quite stable, $Ri \gg \frac{1}{4}$. Note also that in the stratosphere there are only three narrow regions where $Ri < 2$. This result may be modified when more detailed data are available.

5. Spatial Frequency Analysis of Wind Profiles

As mentioned earlier, the turbulent energy spectrum[5] (obtained from spectral analysis of wind profiles) can be used for estimates of diffusivity as well as for other information relating to turbulence (e.g., the energy dissipation rate, and the presence of an inertial subrange, etc.). In general, higher values of energy at the high wave number end of the spectrum should tend to indicate higher amounts of mixing.

In order to characterize the energy spectra derived from the vertical velocity profiles, the A and n parameters of the following equation were determined by least-square fit§:

$$\log P = A - n\log(f) \tag{5}$$

using data from frequency 5 up to half the Nyquist frequency, f_N. At higher frequencies, noise effects dominate the results.¶

An alternate form of Eq. (5) is

$$P(f) = P(1)f^{-n} \tag{6}$$

where $P(1)$ is the energy density per unit mass at frequency 1 extrapolated from the $f = 5$ to $f_N/2$ fitted data. The exponent n characterizes the spectrum. For example if a wind profile yielded $n \sim \frac{5}{3}$, we would most likely have turbulent winds that are isotropic and which have an inertial subrange of turbulence in that region.**

First we spectral analyzed entire trails. Figure 10 shows one of the Miller and Henry smoke trail velocity profiles illustrating the "raw data" before spectral analysis. In addition, this figure shows two synthetic profiles generated with exponents $n = 2$ and $n = 3$. By inspection it is evident that the n of the observed profile lies between the two synthetic profiles.

Since the smoke trails made in Feb. 1973 were not yet reduced to wind profiles, we examined two groups of data: 2 Jimsphere trails on Feb. 13, and 20 NASA trails.[1] All of these trails were in the 5 km to 18 km altitude range and were measured at 25 m spacing, providing 512 data points, with $f_N = 256$ (50 m). Our analysis showed the 20 trails to have $n = 2.75 \pm 0.1$, and no such n's were found below 2. (This is for the range $f = 5$ to $f_N/2$, or 3600 m to 100 m). Similar results were found by other workers. For example, Collis et al.[13] found $n = 3$, and Fichtl et al.[14] found values of n, $2.47 < n < 2.70$. Mather[15] also noted such values of n in the lower wave number part of the spectra (he observed inertial ranges for the higher wave number end) and he associated such large negative slopes (n) with the "buoyancy subrange."[5] He also pointed out that further study is needed before one can conclude that this type of turbulence is the mechanism. Since at the altitude of interest here, most of the winds are predominantly laminar, it would seem that turbulence (in the usual sense) would not be involved in the mechanism.

One relatively well accepted picture of turbulence in the stratosphere characterizes it as occurring in thin horizontal patches presumably brought about by the so-called Kelvin-Helmholtz instability (i.e., a combination of high shear across a statically stable horizontal layer of fluid in a gravitational field). Briefly, when the Richardson number is below $\frac{1}{4}$, a gravitational wave of wavelength $7.5h$ (where h is the thickness of the layer) builds up until it breaks and goes into turbulence. Can spectra be used to detect such patches? The answer is affirmative; one should look for the inertial range value of $n = \frac{5}{3}$.

Analysis of segments of the trails by spectral decomposition was performed on 1.6 km lengths of the original trails to search for possible "local" inertial ranges. Again we restricted the frequency range to $f = 5$ to $f_N/2$ (300–100 m wavelengths). In this group of 160 samples (8 heights × 20 trails), the same mean n was obtained ($n = 2.75$), but fully 20% of the samples had exponents below 2.2, and might be considered to show inertial subranges.

As a matter of prudence, we checked this mathematical procedure by generating a group of 20 synthetic trails with "a spectral exponent" n of 2.8 for 12.8 km long profiles. These synthetic trails matched the real trails in the full-trail analysis, and surprisingly *also* in the segmented analysis. In other words, about 20% of the 1.6 km blocks showed exponents below 2.2. Thus the standard deviation of the exponent widens as the trail length analyzed decreases, and selected regions indeed had exponents consistent with an inertial subrange of turbulence. This finding must be considered when one interprets the above-mentioned experimental results. While the latter are *consistent* with the possible presence of thin turbulent layers, they could not be conclusive evidence for their presence on the basis of this information alone. In other words, caution is needed here.

Our analyses of the Jimsphere data showed that maximum shears increased with altitude from 0.03 $\sec^{-1}$ at 7 km to 0.05 $\sec^{-1}$ at 17 km. Amplitude and Richardson number also increased with altitude. In contrast, the exponent n showed no significant altitude dependence. Furthermore, the Richardson number showed no significant correlation with exponent n (one would expect it to be < 2.2 when $Ri < \frac{1}{4}$). In other words, in the 160 samples 30% showed Richardson number values below 0.25,

§ This form is employed because each turbulence subrange[5] (inertial, buoyancy, viscous convective, etc.) is characterized by the parameter n.

¶ In all our trail analyses, we limited ourselves to frequency ranges below $f_N/2$ in order to avoid noise artifacts. The latter were treacherous because (as will be shown elsewhere) they could sometimes "imitate" inertial ranges reasonably well.

** The term "inertial range" refers to a turbulent condition where there is a range of eddy sizes in which the major portion of "energy input" to a given eddy is from larger eddies and in which most of the energy output is from dissipation to smaller eddy sizes with negligible viscosity effects. This is the famous "energy cascade" effect.

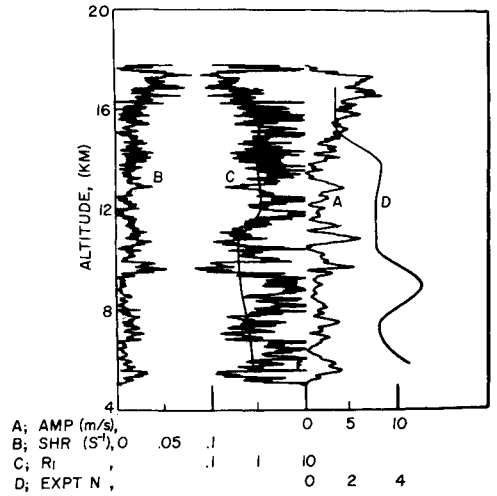

Fig. 11 Analysis of one observed profile: amplitude, shear, Richardson number, and exponent, n, as a function of altitude.

and 20% showed n below 2.2, but no correlation between the two was evident from the data. Figure 11 shows such an analysis for one of the trails. It should be noted that in this analysis, the Ri were obtained from model atmospheres and the more detailed measurement of winds together with simultaneous temperature measurements now in progress should result in the theoretically predicted correlations. In any event, this finding adds further indication for caution.

A technical summary of our spectral analysis procedure is the following: each 64 point sample was 1) prewhitened[16] (a method of processing data which avoids "leakage" artifacts in the computation of spectra), 2) Fourier transformed, 3) corrected for prewhitening, 4) multiplied by f^m (see Fig. 12) where m was the estimated power dependence, 5) smoothed by a tapered weighted average over a 20% frequency bandwidth, and 6) least square fitted for Eq. (5) over the range $\lambda = 300$ m to 100 m, the latter λ corresponding to the $f_N/2$. Parameter values for Eq. (5) were $\log P(1) = 0$, and $n = 2.8$. Standard deviations were 0.8 for 160 samples. The standard error for the mean exponent was 0.05 both for 20 whole trails and 160 trail segments.

Conclusions

Tracer trails gave a value for turbulent diffusivity in the 20 km region of about 0.7 m^2/sec. Spectral analysis of wind profiles gave $n = 2.8$ in agreement with the findings of others and reminiscent of the "buoyancy subrange" type of spectrum. Spectral evidence in 20% of the profile segments suggested the presence of thin turbulent patches (clear air turbulence) in the 5–18 km height range, but the lack of correlations with Ri, and simulation studies with synthetic spectra both suggest the need for caution on this interpretation of the data. Finally we found that shear and amplitude both increased with altitude in this region.

Appendix: Wind Profile Spectral Analysis and Estimation of Turbulent Diffusivity

Zimmerman and Loving[17] have described a method for deriving a lower bound estimate of turbulent diffusivity, K, directly from spectral data under the conditions that there is a high frequency inertial range. Since this information is not yet easily accessible, we give a brief outline of the theory and procedure here. The spectrum (energy density per unit mass of the velocity field, $P(k)$) is related to $K(k_1)$ (the diffusivity produced by turbulence beginning at the lowest wavenumber, k_1) by[18]

$$K(k_1) = C_1 \int_{k_1}^{\infty} dk \left(\frac{P(k)}{k^3}\right)^{1/2} \tag{A1}$$

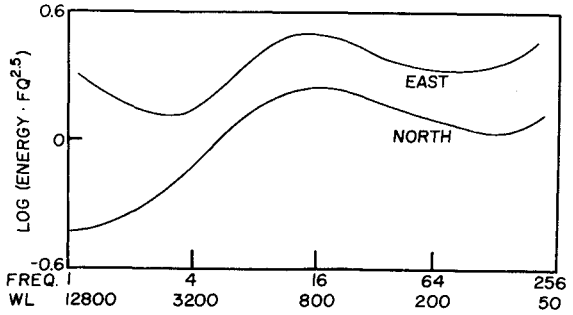

Fig. 12 Spatial frequency spectra of total wind profiles (Miller-Henry 20 trails) with ordinate in arbitrary units.

In the inertial range one has[5]

$$P(k) = \alpha \varepsilon^{2/3} k^{-5/3} \tag{A2}$$

where ε is the dissipation rate and α is a constant. Inserting Eq. (A2) into Eq. (A1) and integrating, we obtain

$$K(k_1) = \alpha^{1/2} C_1 \varepsilon^{1/3} k_1^{-4/3} \tag{A3}$$

where k_1 is the smallest k in the inertial range, and ε is obtained from Eq. (A2). The estimate of k_1 is obtained[17] from a theory which assumes that the inertial range is limited by buoyancy. The lower estimate[19] for k_1 obtained in this way is

$$k_1 = C \varepsilon^{-1/2} N^{3/2} \tag{A4}$$

where N is the buoyancy frequency. Zimmerman and Loving estimated that $\alpha \sim 0.5$, and it is assumed that $C_1 = 1$. Using Eq. (A1) in conjunction with Eq. (A2) to Eq. (A4) one can estimate a lower bound on K. Their paper describes several limitations of the technique.

As a result of the reasons for caution regarding the "inertial ranges" found here and mentioned previously, we postponed the determination of K in this manner until the more detailed data are analyzed.

References

[1] Miller, R. W., Henry, R. M., and Rowe, M. G., "Wind Velocity Profiles Measured by the Smoke-Trail Method at Wallops Island, Virginia (1959–1962)," TN D-2937, 1965, NASA, also TN D-4365, 1968, NASA.

[2] Olsen, R. O., Randhawa, J. S., and Williams, B. H., "Coordinated Measurements of Atmospheric Parameters at Stratospheric Levels," AIAA Paper 73-526, Denver, Colo., 1973.

[3] Golomb, D. and MacLeod, M. A., "Diffusion Coefficients in the Upper Atmosphere from Chemiluminous Trails," *Journal of Geophysical Research*, Vol. 71, No. 9, 1966, pp. 2299–2305.

[4] Rosenberg, N. W., "Application of a Computer-Controlled Two-Dimensional Densitometer to Photograph Chemical Releases," AFCRL TR-73-0155, March 1973, Air Force Cambridge Research Laboratories, Bedford, Mass.

[5] Tennekes, H. and Lumley, J. L., *A First Course in Turbulence*, M.I.T. Press, Cambridge, Mass., 1972, pp. 118, 264, 286.

[6] Chang, P. K., *Separation of Flow*, Pergamon Press, Oxford, 1970, pp. 382–382b.

[7] Schlichting, H., *Boundary Layer Theory*, McGraw-Hill, New York, 1968, p. 692.

[8] Gudiksen, P. H., Fairhall, A. W., and Reed, R. J., "Roles of Mean Meridional Circulation and Eddy Diffusion in the Transport of Trace Substances in the Lower Stratosphere," *Journal of Geophysical Research*, Vol. 73, No. 14, 1968, pp. 1461–1473.

[9] Hoshizaki, H., Conti, R. J., Andersen, L. B., Redler, K. O., Meyer, J. W., McLean, W. J., and Cassady, A. E., "Study of High-Altitude Aircraft Wake Dynamics," Final Report: Task 1, Problem Definition, DOT-TST-90-3, Lockheed Palo Alto Research Lab., Palo Alto, Calif., pp. 2–23.

[10] Monin, A. S. and Yaglom, A. M., *Statistical Fluid Mechanics*, MIT Press, Cambridge, Mass., 1971, p. 92.

[11] Woods, J. D., "On Richardson's Number as a Criterion for Laminar-Turbulent-Laminar Transition in the Ocean and Atmosphere," *Radio Science*, Vol. 4, 1969, pp. 1289–1298.

[12] Turner, J. S., *Buoyancy Effects in Fluids*, Cambridge University Press, Cambridge, England, 1973, pp. 91–126.

[13] Collis, R. T. H., Endlich, R. M., and Mancuso, R. L., "Recent Studies Related to Clear Air Turbulence," *Clear Air Turbulence and*

Its Detection, edited by Y.-H. Pao and A. Goldburg, Plenum Press, New York, 1969, p. 371.

[14] Fichtl, G. H., Camp, W., and Vaughan, W. W., "Detailed Wind and Temperature Profiles," *Clear Air Turbulence and Its Detection*, edited by Y.-H. Pao, and A. Goldburg, Plenum Press, New York, 1969, pp. 308–333.

[15] Mather, G. K., "Clear Air Turbulence Research Activities at the National Aeronautical Establishment," *Clear Air Turbulence and Its Detection*, edited by Y.-H. Pao, and A. Goldburg, Plenum Press, New York, 1969, p. 271.

[16] Blackman, R. B. and Tukey, J. W., *The Measurement of Power Spectra*, Dover, New York, 1958.

[17] Zimmerman, S. P. and Loving, N. V., "Turbulent Dissipation and Diffusivities in the Stratosphere," *CIAP Monograph*, Vol. 1: The Natural Stratosphere, Appendix D-2, 1973.

[18] Hinze, J. O., *Turbulence*, McGraw-Hill, New York, 1959, p. 192.

[19] Phillips, O. M., "On the Bolgiano and Lumley-Shur Theories of the Buoyancy Subrange," *Atmospheric Turbulence and Radio Wave Propagation*, Publishing House "Nauka," Moscow, USSR, 1967, p. 121.

AUGUST 1974 AIAA JOURNAL VOL. 12, NO. 8

Coupled Nongray Radiating Flow about Ablating Planetary Entry Bodies

KENNETH SUTTON*
NASA Langley Research Center, Hampton, Va.

A method of solution for the fully coupled radiating gas flow about an ablating, planetary entry body is developed and applied to Venusian entries. The method couples an inviscid flow solution and a boundary-layer solution (laminar or turbulent) in which the divergence of the radiative flux is included in the energy equation for the solution of each gas layer. The treatment of radiation includes molecular band, continuum, and line transitions with a detailed frequency dependence of the absorption coefficient. Results are presented at typical conditions for unmanned, scientific probes during Venusian entries. These results show that the radiative flux toward the body is attenuated in the boundary layer at downstream regions of the body as well as at the stagnation point and that, even when radiation absorption by ablation products is accounted for, the radiative heating rates along the downstream regions of the body can, under certain conditions, exceed the stagnation-point values. It is also shown that, for Venusian entry, the spectral distribution of radiative flux and the magnitude of radiation absorption by ablation products depend strongly on entry velocity, and that the state of the boundary layer (i.e., laminar or turbulent) can significantly influence the amount of ablation product absorption or emission that occurs in various spectral regions.

Nomenclature

A, B, C, D, E = parameters defined by Eqs. (11–15)
C_2, C_3 = parameters defined by Eqs. (25) and (26)
c_p = specific heat
$\bar{c}_p$ = specific heat parameter defined by Eq. (34)
$\bar{D}$ = self-diffusion coefficient of a reference species
F^R = divergence of radiative flux defined by Eq. (16)
F_j = diffusion factor of jth chemical species
H = total enthalpy, $h+u^2/2$, in Eq. (30)
h = enthalpy
$\bar{h}$ = enthalpy parameter defined by Eq. (34)
j_i = diffusional mass flux of chemical element i
K = body curvature parameter defined by Eq. (19)
$\bar{K}_i$ = mass fraction of chemical element i
k = thermal conductivity
M = molecular weight
m_a = ablation rate of the heat shield
P_1, P_3 = thermodynamic variables defined by Eqs. (20) and (21)
P = pressure
q^C = convective heat flux, see Eq. (33)
q^R = radiative heat flux
Re_θ = momentum thickness Reynolds number for boundary layer
Rn = nose radius of body at $s = 0$, see Fig. 3
r = radial distance from axis of symmetry of body, see Fig. 3
r_b = body radius from axis of symmetry, see Fig. 3
S, Y, T = transformed s, y, t coordinates, defined by Eq. (6)
s, y = body-oriented coordinates, see Fig. 3
$\bar{T}$ = temperature
t = time
u, v = velocity components, see Fig. 3
V_∞ = freestream velocity
V_e = entry velocity
W = weight of entry probe
W/C_dA = ballistic coefficient
$\bar{x}_j$ = mole fraction of chemical species j
$\bar{Z}_j$ = quantity for jth chemical species defined by Eq. (34)
$\bar{Z}_i$ = quantity for ith chemical element defined by Eq. (34)
α_{ij} = mass fraction of chemical element i in chemical species j
β = angle between shock and body, see Fig. 3
γ_e = entry angle
δ = shock standoff distance of inviscid layer
δ^* = boundary-layer displacement thickness defined by Eq. (2)
δ^t = total thickness of shock layer defined by Eq. (1)
θ = body angle, see Fig. 3
θ_c = cone half angle for a spherically capped, conical body
λ = curvature parameter defined by Eq. (17)
λ_δ = value of λ at $y = \delta$, see Eq. (18)
μ = viscosity
μ_1, μ_2 = parameters defined by Eq. (34)
ρ = density
$\rho\varepsilon_d$ = turbulent eddy diffusivity
$\rho\varepsilon_h$ = turbulent eddy conductivity
$\rho\varepsilon_m$ = turbulent eddy viscosity
τ_w = aerodynamic shear at the wall
ϕ = azimuth angle, see Fig. 3

Presented as Paper 73-672 at the AIAA 6th Fluid and Plasma Dynamics Conference, Palm Springs, Calif., July 16–18, 1973; submitted July 31, 1973; revision received February 20, 1974.

Index category: Radiatively Coupled Flows and Heat Transfer.

* Aero-Space Technologist, Gas Radiation Section, Advanced Entry Analysis Branch, Space Systems Division. Member AIAA.